ACS OMEGA

http://pubs.acs.org/journal/acsodf

Article

Enhancement in High-Field J_c Properties and the Flux Pinning Mechanism of ZnO-Buffered MgB_2 Films

Rico Pratama Putra, Jun Yung Oh, Sun Gil Jung, Han Seok Park, Won Nam Kang, and Byeongwon Kang*

Cite This: *ACS Omega* 2023, 8, 11607−11613

Read Online

ACCESS | Metrics & More | Article Recommendations

ABSTRACT: We investigated the flux pinning properties in terms of the critical current density (J_c) and pinning force density (F_p) of MgB_2 films with ZnO buffer layers of various thicknesses. At higher thicknesses of the buffer layer, significantly larger J_c values are observed in the high-field region, whereas J_c values in the low- and intermediate-field regions remain largely unaffected. A secondary point-pinning mechanism other than primary grain boundary pinning is observed in the F_p analysis, which depends on the thickness of the ZnO buffer layer. Moreover, a close relationship between the Mg and B bond ordering and the fitting parameter of secondary pinning is obtained, indicating that the local structural distortion of MgB_2 induced by ZnO buffer layers with different thicknesses may contribute to flux-pinning enhancement in the high-field region. Discovering further advantages of ZnO as a buffer layer other than the delamination resistance it provides will help to develop a MgB_2 superconducting cable with a high J_c for power applications.

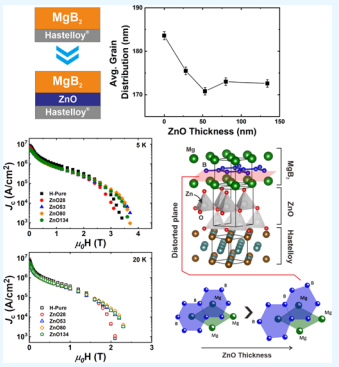

1. INTRODUCTION

Magnesium diboride (MgB_2) has attracted significant attention as a possible replacement for archaic Nb-based superconductors (NbTi, Nb_3Sn, etc.), which continue to be used commercially. MgB_2 has a relatively higher critical temperature (T_c) of ∼39 K[1−3] compared to commercial NbTi, which is known to have a T_c of ∼10 K.[4−6] Furthermore, MgB_2 has been reported to have high upper critical fields (H_{c2}) and high critical current densities (J_c) owing to the absence of weak links.[7−9] Consequently, using MgB_2 is economically advantageous in the applications, where the usage of liquid helium must be avoided. However, despite its relatively high J_c performance, the performance of MgB_2 under magnetic fields remains to be improved.

Several studies have been conducted to enhance the pinning properties of MgB_2 at high magnetic fields by chemical doping,[10−15] grain size reduction,[16−18] and particle irradiation.[19−23] For the thin-film form of MgB_2, various kinds of buffer layers have been tried.[24−29] The use of ZnO as a buffer layer on metallic substrates has yielded promising results. ZnO buffer layers with thicknesses ranging from tens to hundreds of nanometers do not significantly degrade the T_c values while suppressing delamination and hindering unwanted reactions between MgB_2 and the metal substrates.[26,30] As the ZnO buffer layer thickens, the local structure is distorted owing to the atomic bond length variation between Mg−B and Mg−Mg, which leads to the T_c fluctuation. This underlying mechanism of T_c fluctuation has been confirmed by extended X-ray absorption fine structure (EXAFS) measurements.[30] This local structural distortion may introduce additional pinning centers besides the conventional grain boundary pinning[31−33] and affect the pinning behavior of MgB_2.

In this study, we report how ZnO buffer layers affect the magnetic field dependence of the critical current density in MgB_2 films. Increased J_c values were observed at high magnetic fields with no significant change in the collective pinning region. Systematic analyses of the pinning force density (F_p) showed that the thickness of the ZnO buffer layers affects the pinning mechanism in our samples. Furthermore, the relationship between the local structural distortion and the pinning mechanism was carefully studied.

2. EXPERIMENTAL DETAILS

MgB_2 films with mostly *c*-axis-oriented ZnO buffer layers were fabricated on top of a Hastelloy substrate using two separate methods. First, pulsed laser deposition (PLD) was employed to deposit ZnO with thicknesses of 28, 53, 80, and 134 nm, as confirmed by cross-sectional scanning electron microscopy (SEM) measurements. Subsequently, a hybrid physical−chemical vapor deposition (HPCVD) technique was used to deposit the MgB_2 films on the composite ZnO/Hastelloy

Received: February 8, 2023
Accepted: March 7, 2023
Published: March 15, 2023

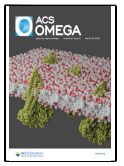

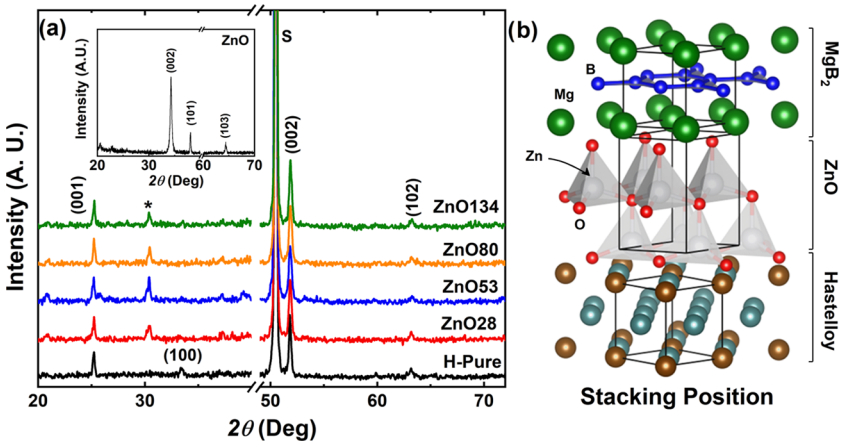

Figure 1. (a) XRD data of MgB_2 films with various thicknesses of ZnO buffer layers. Inset: XRD of the ZnO layer on the Hastelloy substrate and (b) illustration of crystal stacking of MgB_2, ZnO, and Hastelloy substrate.

substrate. To hinder the reaction between the substrate, buffer, and MgB_2 film, the deposition temperature was set to 600 °C, resulting in a ∼1 μm thick buffer layer across all samples.[26,30] The samples corresponding to the thickness of the ZnO buffer layer are denoted as H-pure, ZnO28, ZnO53, ZnO80, and ZnO134, respectively. The crystal structures and surface morphologies of the samples were examined by X-ray diffraction (XRD) and SEM micrographs, respectively.

The magnetic properties of the samples were measured using a Quantum Design MPMS XL at two different temperatures, viz. 5 and 20 K. Both temperatures were selected to match the industry application for a closed-cycle helium cooling system. The samples were aligned with their *ab*-axes perpendicular to the applied magnetic field, and the magnetization loops were recorded with various step sizes (0.01−0.2 T) up to an applied field of 5 T for 5 K and 3 T for 20 K, which is considered to be above the irreversibility field H_{irr} of the samples based on the initial measurement. The critical temperature T_c of each sample was determined by the bifurcation point between the zero-field-cooled (ZFC) and field-cooled (FC) measurements. The critical current density J_c was calculated from the magnetization hysteresis using a simplified Bean's model, $J_c = 20\Delta M/[b(1 - b)3a]$, where ΔM is the height of the $M-H$ loops and a and b ($a > b$) are the lengths of the samples.[34,35]

3. RESULTS AND DISCUSSION

Figure 1a shows the XRD patterns ($\theta-2\theta$ scans) of the MgB_2 films with ZnO buffer layers of various thicknesses on top of the Hastelloy substrate. Sharp (001) peaks are found to be dominant in all samples; however, minor peaks facing other directions are also detected for H-pure, which can be attributed to the lattice mismatch between MgB_2 and the Hastelloy substrate. Applying a ZnO buffer layer underneath the MgB_2 film tends to reduce these peaks. As the ZnO buffer layer increases, the intensities of the (100) and (102) peaks decrease, leading to a better *c*-axis-oriented film. Instead, an impurity peak (marked with *) also appears at approximately 30°, which is assumed to originate from another compound owing to the reaction between MgB_2, ZnO, and Hastelloy in the interlayer region.[26,30] Even though a single ZnO layer has a dominant *c*-axis-oriented peak, as shown in the inset of Figure 1a, no trace of ZnO peaks is observed in the XRD results probably because of the much thicker MgB_2 films. In addition, the *c*-axis lattice parameters calculated from the XRD data are found to be almost identical to a single crystal value of 3.53 ± 0.05 Å. Figure 1b illustrates the three crystal structures of the samples used in this study. Although ZnO has a similar structure to MgB_2, the different in-plane lattice constants between them (MgB_2 ∼3.08 Å, ZnO ∼3.25 Å) may cause internal lattice distortion.[30,36]

The surface morphologies of three representative samples, H-pure, ZnO53, and ZnO134, are presented in Figure 2a−c.

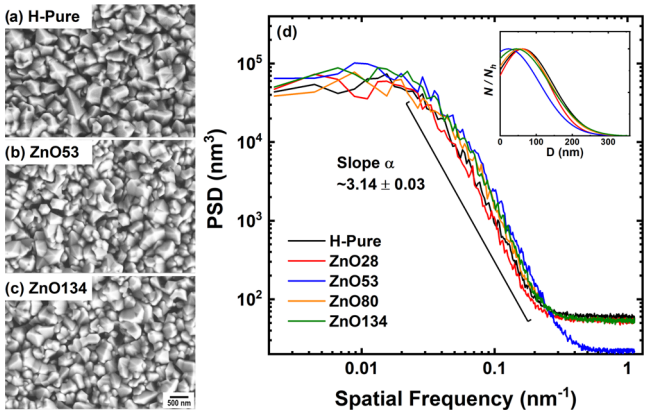

Figure 2. Surface morphology of (a) pure MgB_2, (b) MgB_2 with 53 nm thick ZnO, and (c) 134 nm thick ZnO buffer layer. (d) Power spectral density (PSD) function of all samples deduced from surface morphology data. Inset: Gaussian function of grain size distribution extracted from SEM images.

The three samples exhibit extremely similar surface morphologies in terms of the shape and connectivity of grains, except for the size of grains; the H-pure sample shows a larger grain size compared to those of ZnO53 and ZnO134. To further investigate the grain size distribution, SEM images were obtained using an image-processing method. Eight-bit images were generated in predetermined pixels, subjected to determined pixels, and subjected to color correction and intensity thresholding simultaneously to generate image matrices. The image matrices were analyzed using the power spectra distribution (PSD) function to find the periodicity of surface morphology; the result of the PSD analyses is shown in Figure 2d. The slopes of the double logarithmic functions of PSD, which are related to the growth mode of the samples,

https://doi.org/10.1021/acsomega.3c00809
ACS Omega 2023, 8, 11607−11613

show no significant difference with α values of 3.14 ± 0.03, indicating identical growth conditions for all samples.[37] In contrast, the ZnO53 sample exhibits a distinct feature, despite having a similar slope, it has a longer power law region; thus, it reaches a plateau at a higher frequency of 0.5 nm^{-1}. The higher spatial frequency of the slope and larger area under the PDS function translates to a larger number of grain boundaries in the surface morphology. Furthermore, the grain size distribution was examined based on the pixel density of the image matrices. The normalized Gaussian distributions of the grain size are shown in the inset of Figure 2d, where N and N_h represent the number of particles and the largest number of distribution sizes, respectively. Both results confirm that ZnO53 has the smallest grain size among all samples.

Figure 3 shows the temperature dependence of the normalized susceptibility of ZFC and FC measured at 5 Oe.

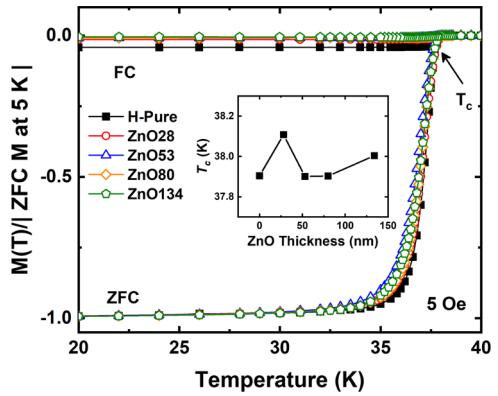

Figure 3. ZFC and FC susceptibility data of MgB_2 films with various thicknesses of ZnO buffer layers measured at 5 Oe. The susceptibility data were normalized with respect to the absolute value of ZFC at 5 K for comparison.

All samples reach perfect diamagnetic states at low temperatures. The T_c values determined by the bifurcation point between ZFC and FC do not decrease as the ZnO layer thickens but rather fluctuate about 38 K, as shown in the inset of Figure 3. The superconducting transitions (ΔT_c) gradually broaden from 3.3 K for H-pure to 3.9 K for ZnO53 without a ZnO thickness dependence. Therefore, we can conclude that ZnO buffer layers with a thickness of up to 134 nm do not degrade the superconducting properties of MgB_2 films.

The field dependences of the calculated J_c at 5 and 20 K are presented in Figure 4a,b, respectively. The self-field J_cs of all samples are observed to be 6−8 × 10^6 A/cm^2 at both temperatures, which is comparable with the previously reported results on Al_2O_3 substrates.[25] Moreover, a positive effect of the ZnO buffer layer on J_c was clearly observed in the high-field region. ZnO buffer layers thicker than 28 nm produced an enhancement in J_c in high magnetic fields. Although this trend was observed at both temperatures, the enhancement was more pronounced at 20 K.

Figure 4c,d shows the double-logarithmic plots of J_c−H to examine the flux pinning property in the intermediate field region, where the vortices are pinned collectively by the relation $J_c \propto H^{-\beta}$, where β represents the effectiveness of pinning. As shown in Figure 4c,d, the fitting results for all samples at both temperatures reveal no significant difference with the ZnO thickness having β of ∼0.96 for 5 K and ∼0.78 for 20 K, indicating a weak collective pinning mechanism.[38,39] These results directly contradict those of SiC-buffered MgB_2. The SiC buffer layer produced a systematic decrease in the β values with respect to the thickness at both temperatures, along with degradation of the J_c values.[33] These comparative results indicate that the flux pinning properties of MgB_2 vary depending on the buffer layer underneath MgB_2.

To study the effect of the ZnO buffer layer on the flux pinning mechanism of MgB_2, we analyzed the pinning force

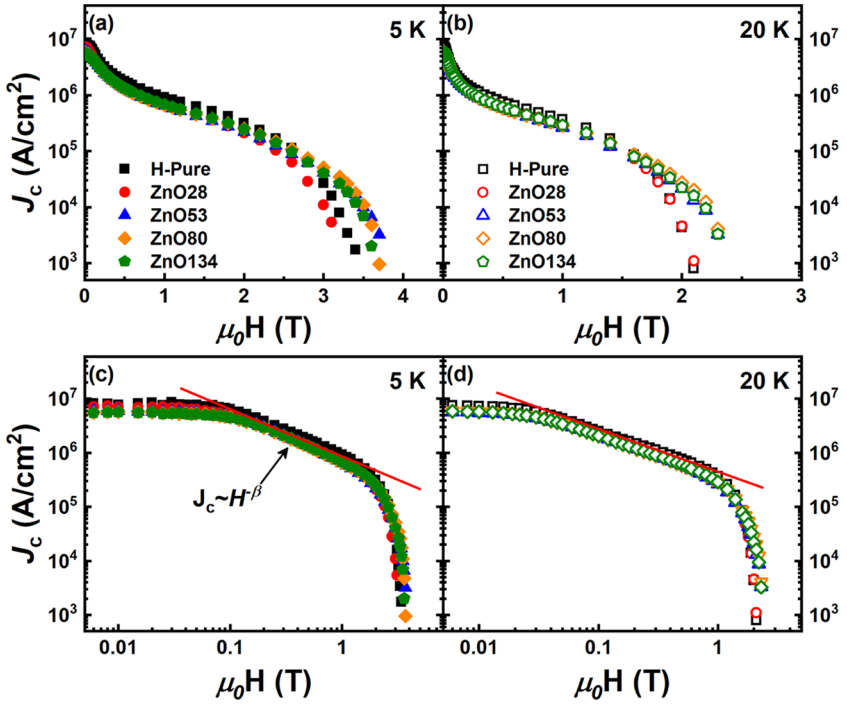

Figure 4. Magnetic field dependences of the critical current density (J_c) as a log−linear scale at (a) 5 K and (b) 20 K and as a log−log scale at (c) 5 K and (d) 20 K.

https://doi.org/10.1021/acsomega.3c00809
ACS Omega 2023, 8, 11607−11613

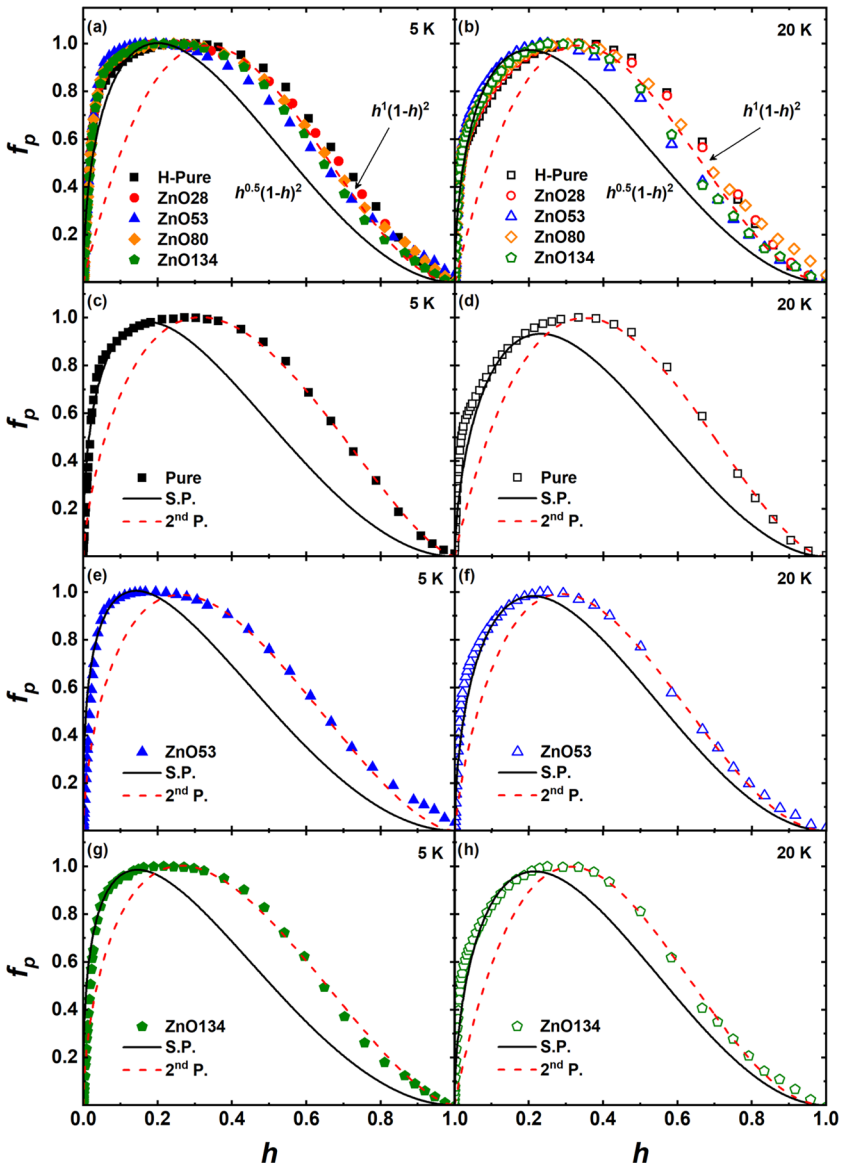

Figure 5. Normalized pinning force density as a function of reduced field of all samples at (a) 5 K and (b) 20 K. Two fitting functions (black solid line for surface pinning and red dotted line for secondary pinning) employed from the Dew-Hughes model for (c) pure sample at 5 K, (d) pure sample at 20 K, (e) ZnO53 at 5 K, (f) ZnO53 at 20 K, (g) ZnO134 at 5 K, and (h) ZnO134 at 20 K.

density F_p deduced from J_c (H) data at 5 and 20 K using the relation of $F_p = J_c \times \mu_0$ H. Figure 5a−h shows the magnetic field dependence of the normalized flux pinning force $f_p = F_p/F_{p,max}$ as a function of the reduced field $h = H/H_{irr}$ at 5 and 20 K, where $F_{p,max}$ is the maximum pinning force density and H_{irr} is the irreversible field determined from the linear extrapolation of the Kramer scaling, where the value of $J_c^{0.5}$ $H^{0.25}$ tends to zero.[40,41] The f_p behaviors of all samples can be expressed by the formula $f_p = Ah^p(1 - h)^q$, where A is an independent parameter of the applied field, and p and q are parameters describing the actual pinning mechanism.[40]

The dominant pinning mechanism of the MgB_2 film is known to be grain boundary pinning, which is classified as a volume surface pinning mechanism.[7,40] The normalized F_p values for all of the samples at both temperatures are shown in Figure 5a,b, respectively, and a broad plateau is observed in all of the samples. An original pinning function for grain boundary (surface) pinning was employed using fixed values of $p = 0.5$ and $q = 2$ (black line) to fit the data points. The result of the fitting appears to be effective in covering only the low-field region. This inefficacy in fitting leads to the assumption that an additional pinning source was applied to the high-field region. As a preliminary premise, we assume that secondary pinning acts as a point pinning originating from the distortion in the MgB_2 matrix caused by lattice mismatch, crystal distortion, or incomplete grain growth. Based on this premise, a trial function with default values of $p = 1$ and $q = 2$ was used for point pinning; the results are presented as dashed red lines. The results shown are a relatively good fit; however, not all data points in the high-field region can be covered, which implies that the fitting values must be modified. Modification of the fitting values for the secondary pinning function may help us understand the origin of the additional pinning centers caused by the ZnO buffer layers.

The modified dual pinning method is presented for three representative samples of H-pure, ZnO53, and ZnO134 at 5 and 20 K, as shown in Figure 5c−h. Qualitatively, the pure sample at 5 K exhibits the broadest plateau compared with the

https://doi.org/10.1021/acsomega.3c00809
ACS Omega 2023, 8, 11607−11613

Table 1. Fitting Results of the β Value from the Log−Log Scale in Relation with $J_c \propto H^{-\beta}$, p Values on 1st and 2nd Pinning at Two Temperatures 5 and 20 K with Fixed q = 2 and Normalized Mg−B Fourier Transform Intensity (I_{Mg-B}/I_{Mg-Mg})

sample name	temperature						intensity $\left(\frac{I_{Mg-B}}{I_{Mg-Mg}}\right)$
	5 K			20 K			
	β-value (±0.05)	1st pinning p (±0.02)	2nd pinning p (±0.02)	β-value (±0.05)	1st pinning p (±0.02)	2nd pinning p (±0.02)	
pure	0.92	0.42	1.30	0.76	0.56	1.14	0.99
ZnO28	0.96	0.41	1.10	0.77	0.55	1.10	0.94
ZnO53	1.00	0.33	0.80	0.78	0.53	0.80	0.81
ZnO80	0.95	0.34	1.00	0.82	0.54	1.00	0.75
ZnO134	0.95	0.34	0.90	0.76	0.55	0.98	0.73

others. As the buffer layer thickness increases to 53 nm, the plateau of f_p became narrower than that of H-pure. As the ZnO buffer layer thickens further, the plateau becomes even broader, as shown in Figure 5e. Similar behavior is observed in the data at 20 K. For a quantitative study, individual fitting with a fixed value of q = 2 on the data in the low-field region was performed, for which the p values at both temperatures are listed in Table 1. The p values show a gradual decrease with the ZnO thickness at 5 K and remain constant at 20 K. Similar approaches with a fixed value of q = 2 were used for secondary pinning in the high-field region, for which the fitting results are listed in Table 1. The p values at both temperatures show a decreasing trend with increasing ZnO thickness with a larger variation at 5 K. These fitting results show that the secondary pinning is a point-like pinning mechanism. However, the application of the ZnO buffer layer resulted in a mixture of pinning mechanisms depending on the thickness of the ZnO layer.

The ZnO53 sample, in contrast, exhibits significant discrepancies in terms of shape of f_p and p values. Table 1 shows that ZnO53 exhibits the smallest p values at both temperatures. Moreover, in contrast to the other samples, the f_p data of ZnO53 can be fitted by a single pinning mechanism with p and q values close to those of surface pinning. This special behavior can be attributed to the minimization of grain size by grain boundary pinning.[17,18]

However, determining the origin of the secondary pinning of samples is challenging. The surface condition and grain size distribution alone cannot explain the behaviors of J_c and F_p. Local structure studies using Raman spectra and EXAFS measurements have revealed the presence of local lattice distortion in MgB_2 films owing to the application of a ZnO buffer layer.[26,30] While the Mg−Mg bond ordering showed insignificant fluctuation, the Mg−B bond ordering was found to be heavily affected by the ZnO thickness.[30] To find a correlation between the local structure distortion and the second pinning mechanism, renormalization of the Fourier transform of the Mg−B bond ordering with respect to the Mg−Mg bond ordering was measured by Mg K-edge EXAFS, for which the results are shown in Figure 6a.[42−46] Renormalization to the Mg−Mg bond was proposed to reduce the probability of miscalculation caused by the backscattering process and other disturbances. Based on the assumption that the local structural distortion affects the secondary pinning behavior, the p values of the pinning functions are plotted as a function of the relative bond ordering in Figure 6b. Systematic decreases in the p values followed by a decrease in the Mg−B bond ordering are observed at both temperatures. With the exception of ZnO53, the Mg−B bond ordering in the local

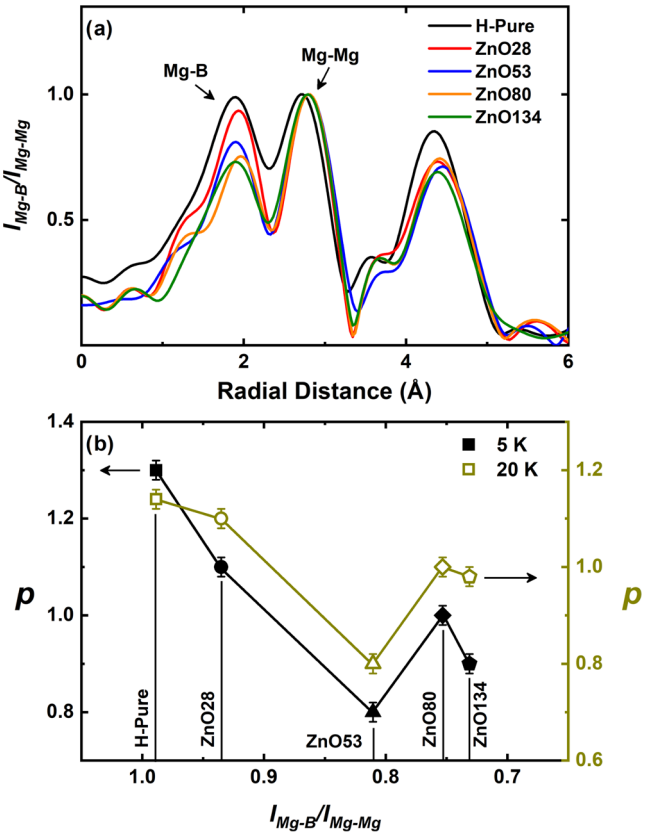

Figure 6. (a) Normalized intensity of MgB_2 EXAFS Fourier transform with respect to the second shell Mg−Mg bond intensity. (b) Relation between ZnO thickness and the p value of secondary pinning as a function of the normalized Mg−B bond intensity.

structure of MgB_2 contributes to the secondary pinning centers. Furthermore, the abrupt change in the p value of ZnO53, which gives it a distinctive feature, may be mainly due to the grain boundary effect rather than the local structure distortion.

Although the correlation between the local structure and the secondary pinning center is noticeable, our investigation is limited. Because the thickness of MgB_2 is ∼1 μm, the local structural distortion induced by the lattice mismatch between ZnO and MgB_2 may not be uniform across the thickness and surface of the films. Therefore, another pinning source may exist. Nevertheless, our results indicate that the local structural distortion generated in the ZnO-buffered MgB_2 films can serve as an additional pinning center, which can significantly enhance the flux pinning properties under high magnetic fields.

https://doi.org/10.1021/acsomega.3c00809
ACS Omega 2023, 8, 11607−11613

4. CONCLUSIONS

The flux pinning properties in terms of the J_c and F_p behaviors of MgB_2 films with ZnO buffer layers of various thicknesses were studied. While all samples exhibited similar behavior in the low- and intermediate-field regions, significant enhancement of the J_c values was observed in the high-field region, indicating that the ZnO buffer layers contribute to the additional pinning centers to enhance the flux pinning properties. The secondary pinning, in addition to the primary grain boundary pinning, was found to be a point-like pinning mechanism, which depends on the ZnO thickness, as shown by various p values of fitting. Furthermore, the Mg and B bond ordering and p values were found to be closely correlated, which indicates that the local structural distortion induced by the ZnO buffer layer contributes to the flux-pinning enhancement in the high field. Considering the advantages of the ZnO buffer layer in improving the J_c and F_p in addition to reducing delamination, MgB_2 films with high J_c in high fields can be developed, which is needed for power applications.

AUTHOR INFORMATION

Corresponding Author

Byeongwon Kang − *Department of Physics, Chungbuk National University, Cheongju 28644, South Korea;* orcid.org/0000-0002-5491-8410; Email: bwkang@chungbuk.ac.kr

Authors

Rico Pratama Putra − *Department of Physics, Chungbuk National University, Cheongju 28644, South Korea*

Jun Yung Oh − *Department of Physics, Chungbuk National University, Cheongju 28644, South Korea*

Sun Gil Jung − *Department of Physics, Sungkyunkwan University, Suwon 440 746, South Korea;* Present Address: Department of Physics Education, Suncheon National University, Suncheon, 57922, South Korea

Han Seok Park − *Department of Physics, Chungbuk National University, Cheongju 28644, South Korea*

Won Nam Kang − *Department of Physics, Sungkyunkwan University, Suwon 440 746, South Korea*

Complete contact information is available at: https://pubs.acs.org/10.1021/acsomega.3c00809

Notes

The authors declare no competing financial interest.

ACKNOWLEDGMENTS

This study was supported by the Basic Science Research Program of the National Research Foundation of Korea (NRF), which is funded by the Ministry of Education (2021R1I1A3044518).

REFERENCES

(1) Nagamatsu, J.; Nakagawa, N.; Muranaka, T.; Zenitani, Y.; Akimitsu, J. Superconductivity at 39 K in magnesium diboride. *Nature* **2001**, *410*, 63.

(2) Kortus, J.; Mazin, I. I.; Belashchenko, K. D.; Antropov, V. P.; Boyer, L. L. Superconductivity of Metallic Boron in MgB_2. *Phys. Rev. Lett.* **2001**, *86*, 4656.

(3) Choi, H. J.; Roundy, D.; Sun, H.; Cohen, M. L.; Louie, S. G. The origin of the anomalous superconducting properties of MgB_2. *Nature* **2002**, *418*, 758.

(4) Lubell, M. S. Empirical Scaling Formulas for Critical Current and Critical Field for Commercial NbTi*. *IEEE Trans. Magn.* **1983**, *19*, 754.

(5) Vinod, K.; Kumar, R. G. A.; Syamaprasad, U. Prospects for MgB_2 superconductors for magnet application. *Supercond. Sci. Technol.* **2007**, *20*, R1−R13.

(6) Patel, D.; Matsumoto, A.; Kamakura, H.; Moronaga, T.; Hara, Y.; Hara, T.; Maeda, M.; Hossain, M. S. A.; Yamauchi, Y.; Choi, S.; Kim, J. H. Superconducting Joining Concept for Internal Magnesium Diffusion-Processed Magnesium Diboride Wires. *ACS Appl. Mater. Interfaces* **2021**, *13*, 3349.

(7) Larbalestier, D. C.; Cooley, L. D.; Rikel, M. O.; Polyanskii, A. A.; Jiang, J.; Patnaik, S.; Cai, X. Y.; Feldmann, D. M.; Gurevich, A.; Squitieri, A. A.; Naus, M. T.; Eom, C. B.; Hellstrom, E. E.; Cava, R. J.; Regan, K. A.; Rogado, N.; Hayward, M. A.; He, T.; Slusky, J. S.; Khalifah, P.; Inumaru, K.; Haas, M. Strongly linked current flow in polcrystalline forms of superconductors MgB_2. *Nature* **2001**, *410*, 186.

(8) Zhuang, C.; Tan, T.; Wang, Y.; Bal, S.; Ma, X.; Yang, H.; Zhang, G.; He, Y.; Wen, H.; Xi, X. X.; Feng, Q.; Gan, Z. Clean MgB_2 thin films on different type of single-crystal substrate fabricated by hybrid physical-chemical vapor deposition. *Supercond. Sci. Technol.* **2009**, *22*, No. 025002.

(9) Abrikosov, A. A. On the Magnetic Properties of Superconductor of the Second Group. *Sovi. Phys. JETP* **1957**, *5*, 1174−1182.

(10) Angst, M.; Bud'ko, S. L.; Wilke, R. H. T.; Canfield, P. C. Difference between Al and C doping in anisotropic upper critical field development in MgB_2. *Phys. Rev. B* **2005**, *71*, No. 144512.

(11) Wang, J. L.; Zeng, R.; Kim, J. H.; Lu, L.; Dou, S. X. Effects of C substitution on the pinning mechanism of MgB_2. *Phys. Rev. B* **2008**, *77*, No. 174501.

(12) Pogrebnyakov, A. V.; Xi, X. X.; Redwing, J. M.; Vaithyanathan, V.; Schlom, D. G.; Soukiassian, A.; Mi, S. B.; Jia, C. L.; Giencke, J. E.; Eom, C. B.; Chen, J.; Hu, Y. F.; Cui, Y.; Qi, Li. Properties of MgB_2 thin films with carbon doping. *Appl. Phys. Lett.* **2004**, *85*, 2017.

(13) Dou, S. X.; Soltanian, S.; Horvat, J.; Wang, X. L.; Zhou, S. H.; Ionescu, M.; Liu, H. K.; Munroe, P.; Tomsic, M. Enhancement of the critical current density and flux pinning of MgB_2 superconductor by nanoparticle SiC doping. *Appl. Phys. Lett.* **2002**, *81*, 3419.

(14) Karpinski, J.; Zhigadlo, N. D.; Katrych, S.; Rogacki, K.; Batlogg, B.; Tortello, M.; Puzniak, R. MgB_2 single crystal substituted with Li and with Li-C: Structural and supercondcuting properties. *Phys. Rev. B* **2008**, *77*, No. 214507.

(15) Li, W. X.; Li, Y.; Chen, R. H.; Zeng, R.; Dou, S. X.; Zhu, M. Y.; Jin, H. M. Raman study of element doping effects on the superconductivity of MgB_2. *Phys. Rev. B* **2008**, *77*, No. 094517.

(16) Braccini, V.; Gurevich, A.; Giencke, J. E.; Jewell, M. C.; Eom, C. B.; Larbalestier, D. C.; Pogrebnyakov, A.; Cui, Y.; Liu, B. T.; Hu, Y. F.; Redwing, J. M.; Qi, Li.; Xi, X. X.; Singh, R. K.; Gandikota, R.; Kim, J.; Wilkens, B.; Newman, N.; Rowell, J.; Moeckly, B.; Ferrando, V.; Tarantini, C.; Marre′, D.; Putti, M.; Ferdeghini, C.; Vaglio, R.; Haanappel, E. High-field superconductivity in alloyed MgB_2 thin films. *Phys. Rev. B* **2005**, *71*, No. 012504.

(17) Martinez, E.; Mikheenko, P.; Marinez-Lopez, M.; Millan, A.; Bevan, A.; Abell, J. S. Flux pinning foce in bulk MgB_2 with variable grain size. *Phys. Rev. B* **2007**, *75*, No. 134515.

(18) Mikheenko, P.; Martinez, E.; Bevan, A.; Abell, J. S.; MacManuss-Driscoll, J. L. Grain boundaries and pinning in bulk MgB_2. *Supercond. Sci. Technol.* **2007**, *20*, S264.

(19) Bugoslavsky, Y.; Cohen, L. F.; Perdins, G. K.; Polichetti, M.; Tate, T. J.; Gwilliamss, R.; Caplin, A. D. Enhancement of the high-magnetic-field critical current density of superconducting MgB_2 by proton irradiation. *Nature* **2001**, *411*, 561.

(20) Pallecchi, I.; Tarantini, C.; Aebersold, H. U.; Braccini, V.; Fanciulli, C.; Ferdeghini, C.; Gatti, F.; Lehmann, E.; Manfrienetti, P.; Marre, D.; Palenzona, A.; Siri, A. S.; Vignolo, M.; Putti, M. Enhanced flux pinning in neutron irradiated MgB_2. *Phys. Rev. B* **2005**, *71*, No. 212507.

(21) Talapatra, A.; Bandyopadhyay, S. K.; Sen, P.; Banerjee, A.; Rawat, R. Magnetization measurements of neon ion irradiated MgB_2 superconductors. *Supercond. Sci. Technol.* **2007**, *20*, 1193.
(22) Jung, S.-G.; Pham, D.; Han, Y-S.; Lee, J. M.; Kang, W. N.; Kim, C.; Yeo, S.; Jun, B.-H.; Park, T. Improvement of bulk supercondcuting current capability of MgB_2 film using surface degradation. *Scr. Mater.* **2022**, *209*, No. 114424.
(23) Jung, S. G.; Pham, D.; Lee, J. M.; Han, Y-S.; Kang, W. N.; Park, T. Effects of surface damage on critical current density in MgB_2 thin films. *Curr. Appl. Phys.* **2021**, *22*, 14.
(24) Putri, W. B. K.; Tran, D. H.; Kang, B.; Lee, N. H.; Kang, W. N.; Oh, S. J. Enhancement in High-Field Jc Properties and the Flux Pinning Mechanism of MgB_2 Thin Films on Crystalline SiC Buffer Layers. *J. Supercond. Novel Magn.* **2014**, *27*, 401.
(25) Pham, D.; Ngoc, H. V.; Jung, S. G.; Kang, D. J.; Kang, W. N. Enhanced critical current density of MgB_2 thin films deposited at low temperatures by ZnO seed impurity. *Curr. Appl. Phys.* **2018**, *18*, 762.
(26) Putra, R. P.; Lee, Y. S.; Duong, P.; Ko, Y. J.; Kang, W. N.; Kim, K.-H.; Kang, B. Electron-phonon coupling behavior in MgB_2 films with various thicknesses of ZnO buffer layer on metallic substrates. *Solid State Commun.* **2021**, *323*, No. 114117.
(27) Putri, W. B. K.; Kang, B.; Duong, P.; Kang, W. N. Reducing delamination in MgB_2 films deposited on Hastelloy tapes by applying SiC buffer layers. *Thin Solid Films* **2015**, *590*, 80.
(28) Nishida, A.; Taka, C.; Chromic, S. Scaling analyses on the critical current density in MgB2/SiC/Si thin film processed at higher temperature. *Mater. Sci. Eng.* **2019**, *502*, No. 012184.
(29) Nishida, A.; Taka, C.; Chromic, S. Scaling analyses on the critical current density in MgB_2/NbN/Si thin film. *J. Phys. Conf.* **2020**, *1559*, No. 012041.
(30) Putra, R. P.; Lee, Y. S.; Oh, J. Y.; Tien, L. M.; Kang, W. N.; Miyanaga, T.; Kang, B. Correlation between Tc and local structure of MgB_2 with ZnO buffer layer: X-Ray absorption fine structure study. *Physica B+C* **2022**, *645*, No. 414234.
(31) Kitaguchi, H.; Matsumoto, A.; Kumakura, H.; Kitamura, H.; Doi, T.; Yamamoto, H.; Yamamoto, H.; Saitoh, K.; Saitoh, K.; Sosiati, H.; Sosiati, H.; Hata, S. MgB_2 films with very high critical current densities due to strong grain boundary pinning. *Appl. Phys. Lett.* **2004**, *85*, 2842.
(32) Jung, S.-G.; Seong, W. K.; Kang, W. N. Effect of columnar grain boundary on flux pinning in MgB_2 films. *J. Appl. Phys.* **2012**, *111*, No. 053906.
(33) Kang, B.; Putri, W. B. K.; Kang, W. N. Effect of SiC buffer layer on flux pinning property of MgB_2 tapes. *Curr. Appl. Phys.* **2019**, *19*, 670.
(34) Wang, X. L.; Li, A. H.; Yu, S.; Ooi, S.; Hirata, K.; Lin, C. T.; Collings, E. W.; Sumption, M. D.; Bhatia, M.; Ding, S. Y.; Dou, S. X. Thermally assisted flux flow and individual vortex pinning in $Bi_2Sr_2Ca_2Cu_3O_{10}$ single crystals grown by the traveling solvent floating zone technique. *J. Appl. Phys.* **2005**, *97*, No. 10B114.
(35) Bean, C. P. Magnetization of hard superconductos. *Phys. Rev. Lett.* **1962**, *8*, 250.
(36) Reeber, R. R. Lattice parameters of ZnO from 4.2 to 296 K. *J. Appl. Phys.* **1970**, *41*, 5063.
(37) Oh, J. Y.; Song, C. Y.; Ko, Y. J.; Lee, J. M.; Kang, W. N.; Yang, D. S.; Kang, B. Strong correlation between flux pinning and epitaxial strain in GdBa2Cu3O7-x/La0.7Sr0.3MnO3 nanocrystalline heterostructure. *RSC Adv.* **2020**, *10*, 39102.
(38) Blatter, G.; Feigel'man, M. V.; Geshkenbein, V. B.; Larkin, A. I.; Vinokur, V. M. Vortices in high-temperature superconductors. *Rev. Mod. Phys.* **1994**, *66*, 1125.
(39) Dam, B.; Huijbregtse, J. M.; Klaassen, F. C.; Van der Geest, R. C. F.; Doornbos, G.; Rector, J. H.; Testa, A. M.; Freisem, S.; Martinez, J. C.; Stäuble-Pümpin, B.; Griessen, R. Origin of high critical currents in $YBa_2Cu_3O_{7-\delta}$ superconducting thin films. *Nature* **1999**, *399*, 439.
(40) Dew-Hughes, D. Flux pinning mechanisms in type II superconductors. *Philos. Mag.* **1974**, *30*, 293.
(41) Kramer, E. J. Scaling laws for flux pinning in hard superconductors. *J. Appl. Phys.* **1973**, *44*, 1360.
(42) Putri, W. B. K.; Duong, P. V.; Kang, W. N.; Miyanaga, T.; Yang, D. S.; Kang, B. Close relation between Mg−Mg bonds and Tc of SiC buffered-MgB_2 tapes. *J. Alloys Compd.* **2016**, *665*, 352.
(43) Putri, W. B. K.; Tran, D. H.; Lee, O. Y.; Kang, W. N.; Miyanaga, T.; Yang, D. S.; Kang, B. Effect of different thickness crystalline SiC buffer layers on the ordering of MgB_2 films probed by extended x-ray absorption fine structure. *J. Appl. Phys.* **2014**, *115*, No. 093901.
(44) Miyanaga, T.; Kanno, T.; Fujine, Y.; Araaki, J.; Yoshizawa, M. Polarized XAFS study of Mg K-edge for MgB_2 on ZnO. *J. Electron Spectrosc. Relat. Phenom.* **2011**, *184*, 254.
(45) Seo, M.; Miyanaga, T.; Kanno, T. Local Structure Analysis of MgB_2 Thin Films by Polarized XAFS. *e-J. Surf. Sci. Nanotechnol.* **2012**, *10*, 633.
(46) Miyanaga, T.; Matsumura, R.; Seo, M.; Takeda, K.; Hatanaka, D.; Yoshizawa, M. Polarized XAFS Analyses for MgB_2 Thin Films. *J. Supercond. Novel Magn.* **2017**, *30*, 1665.

https://doi.org/10.1021/acsomega.3c00809
ACS Omega 2023, 8, 11607−11613